Front. Phys. China, 2010, 5(2): 131–146
DOI 10.1007/s11467-010-0025-7

REVIEW ARTICLE

Preparation of narrow-band photons for atomic-based quantum memory with a type-I phase matched periodical poled KTP crystal

Bao-sen SHI (史保森)†, **Chang ZHAI** (翟畅), **Fu-yuan WANG** (王福源), **Guang-can GUO** (郭光灿)

Key Laboratory of Quantum Information, University of Science and Technology of China, Hefei 230026, China
E-mail: drshi@ustc.edu.cn

Received April 11, 2010; accepted April 30, 2010

Transferring a quantum state between a photon and a quantum memory is the key point for realizing a long-distance quantum communication, and is also a basic ingredient of linear optical quantum computation. In an atomic-based network, the efficient coupling between a photon and an atomic system is a prerequisite for realizing the transfer of information between them, which requires that the photon should have a comparable bandwidth with the natural bandwidth of an atom. Therefore, generating a narrow-band photon has become a very important topic in the quantum information field. One simple and efficient way is cavity-enhanced spontaneously parametric down-conversion. In this paper, we will review and introduce a series of experiments done in our group for realizing this goal. We believe these works are very useful for the research in this direction.

Keywords quantum memory, narrow-band photons, KTP crystal

PACS numbers 42.50.Dv, 42.50.Gy, 42.65.Ky

Contents

1 Motivation 131
2 Efficient cw violet-light generation in a ring cavity 132
3 Preparation of the photon pair source in a single-pass configuration 134
3.1 Experimental set-up 134
3.2 Experimental results 135
3.3 Discussion 136
4 Generating a multi-mode photon pair with the aid of cavity 137
5 Quantum interference of multi-mode two-photon pairs with a Michelson interferometer 139
6 Experiment measuring the coherence length of the single multi-mode photon 141
7 The generation of a narrow-band photon pair 143
8 Conclusion 145
Acknowledgements 145
References 145

1 Motivation

The goal of quantum information research is to build a quantum network by which any user can communicate with others easily. Such network is expected to play an important role in extending the range of quantum communication and quantum cryptography [1, 2] to long distances. In general, a quantum network consists of spatially separated nodes to store and manipulate quantum information and quantum channels that connect the nodes. A photon can propagate over long distances in free space or in optical fibers and is a robust and efficient candidate. Atoms are well-suited to precise state manipulation and long-lived storage of quantum information in metastable states, and can be isolated from the environment. Therefore, an alkali atomic system, like a hot atomic vapor or a cold atomic cloud of, for example rubidium (Rb) or cesium (Cs) may be a good candidate [3–5]. In an atomic-based network, the efficient coupling between a photon and an atomic system is a prerequisite for realizing the transfer of information between them, which requires that the photon should have a comparable bandwidth with the natural bandwidth of an atom. Spontaneously parametric down-conversion (SPDC) in a nonlinear crystal is the most widely used way for preparing an entangled photon pair so far [6–8], but its loose phase-matching condition sets the constraint of the linewidth of

the generated photon to be on the order of THz [9]. On the contrary, the typical natural linewidth of the atom is on the order of MHz, therefore it is almost impossible to have an efficient coupling between the atom and the photon. Therefore, preparing a narrow-band photon is the key point for realizing an atomic-based network. Besides, a narrow-band photon can be used to study the question of fundamental issues of atom–photon interactions on a single photon. The requirement of narrow band excludes these photon sources such as molecules in solid-state matrices [10], nitrogen-vacancy centers at room temperature [11] and quantum dots [12]. Currently, there are two possible ways for preparing a narrow band photon: one is based on the spontaneous Raman scattering in an atomic ensemble system, which has been used in Refs. [3–5, 13, 14]. Although this method is workable, the experimental effort is high. Another way is based on a resonant optical parametric oscillator (OPO) operated far below threshold, as has been demonstrated in Ref. [15]. This is a relatively easy and efficient way, the photon pair whose frequency matches the cavity mode will be enhanced significantly. It offers an advantage of flexibility concerning the wavelength and bandwidth, therefore several groups, including ours [16–20], recently followed this method to prepare a narrow band photon experimentally. Our group is now involved in the realization of quantum memory based on a cold Rb atomic ensemble (D_2 line at 780 nm) trapped in a magneto–optical trap [13, 21]. We hope to realize the transfer of the quantum state between an atomic ensemble and a narrow-band single photon. In order to realize this goal, we should prepare the narrow-band photon at 780-nm wavelength first. In this paper, we will introduce and review a series of works along this research direction done in our group, and show the differences between the results given by other groups and ours. The outline of this paper is as follows: after we briefly explain our motivation in Section 1, we will introduce the experiment on the efficient generation of cw ultraviolet light at 390-nm wavelength with the aid of ring cavity [22] in Section 2. The output will be used as the pump laser in the succeeding experiments. Then we will show the experimental preparation of an ultra-bright two-photon source in a single-pass SPDC configuration [9] in Section 3. After that, we put the nonlinear crystal in a ring cavity and show an experiment on the preparation of a multi-mode photon pair via a degenerate optical parametric oscillator far below threshold [19] in Section 4. In Section 5 and Section 6, we will characterize the first-order and the second-order coherence properties of the photon generated in Section 4 by performing two interference experiments: one is two-photon interference [23] in Section 5 and the other is single-photon interference [24] in Section 6. In Section 7, we will report on the generation of narrow-band photon pairs by using a spectral filtering cavity [20]. Finally, we will give a brief conclusion in Section 8.

2 Efficient cw violet-light generation in a ring cavity

In our laboratory, the atomic system for quantum memory is rubidium (D_2 line at 780 nm), therefore the wavelength of the narrow-band photon should be 780 nm. The base for this aim is an easily available and powerful cw source of light at 390 nm. We have no such laser, so we have to prepare it first. At present, the commonly used method for getting such a source is to double the frequency of a solid-state laser output. Because there is no high power cw laser at 780 nm in our laboratory, and usually the efficiency of the second harmonic generation (SHG) in a single-pass configuration is very lower, so we have to obtain a strong enough 390-nm laser with the aid of the cavity. Besides, a periodically-poled KTP crystal is used for further improving the conversion efficiency. A periodically-poled crystal, like a periodically-poled Lithium Niobate (PPLN) or a periodically-poled Titanyl Phosphate (PPKTP), with an appropriate grating period, permits efficient three-wave mixing at user-selectable wavelengths by the technique of quasi-phase matching (QPM). QPM allows one to utilize larger nonlinear coefficients in some materials, thus leading to substantially higher two-photon production rates. In this section, we will report on an efficient cw SHG at 780-nm wavelength with a first-order type-I phase matching PPKTP crystal in a ring cavity; the wavelength corresponds to the D_2 line of Rb atom transition. Despite the fact that the theory of the SHG is well established and many realizations of such sources have been reported, our experiment is not trivial owing to the following facts: our fundamental source is a small and relatively cheap grating-stabilized external cavity diode laser (Toptica DL100), and its frequency is locked to the transition line D_2 of Rb^{87} atom (780 nm) by the saturated absorption technique, in contrast with other experiments in which a bigger and more expensive Ti: Sapphire laser is used [25–30]; Second, a type-I phase matching PPKTP crystal is used as the frequency doubling crystal. This is the first experiment performed for realizing SHG at 780 nm in a cavity to our best knowledge, although an SHG experiment at 780-nm wavelength using a single-pass configuration was done several years ago [31]. PPKTP has a relatively large optical nonlinearity and good power-handling capability in the UV and visible spectra, therefore it is attractive for the generation of blue-UV radiation.

The PPKTP crystal is 10-mm long, 1-mm thick and 2-mm wide, and has 2.95-μm poled period. The crystal was bought from Raicol Company. The facets of the crystal were anti-reflection coated at 780 nm and 390

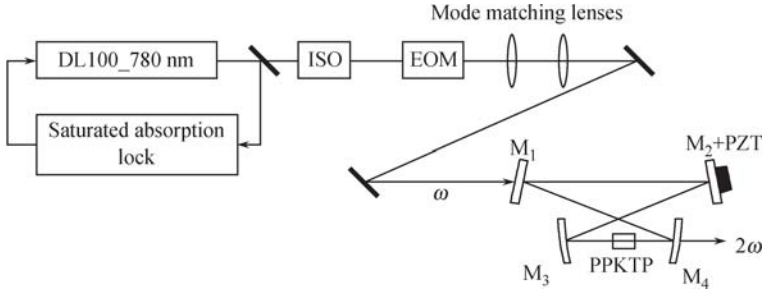

Fig. 1 The schematic drawing of the experimental set-up. DL100_780 nm: laser; ISO: isolator; EOM: electronic optical modulator; M_1, M_2: mirrors; M_3, M_4: mirrors with 80-mm radius of curvature.

nm. The crystal is mounted in a home-made temperature controlled Peltier oven with the stability of ± 0.05°C. We first perform a single-pass SHG experiment to find the optimal temperature at which the crystal works. In this case, a relatively loose focusing condition (focus length: 10 cm) is used in order to avoid the influence of beam divergence. The experimental result shows that the optimal temperature is about 12.5°C. This low temperature introduces the difficulty to our temperature controller because of the relatively large temperature difference between the crystal and the environment (about 21°C). The temperature spectrum is $\Delta T_{\mathrm{FWHN}} = 2.6$ K. From this value, we calculate that the effective length of the crystal is about 3.9 mm using the Eq. (4) of Ref. [25], which is quite smaller compared with the actual physical length of 10 mm. The derivatives of the refractive indices with the temperature at the fundamental and the second harmonic wavelengths used in calculation are obtained at the phase matching temperature T_0 from Ref. [32]. Here, we have to say that the value of the effective length is only a reference because there are no Sellmerier equations which are valid for a wavelength shorter than 450 nm and we assume that Sellmerier equations of Ref. [33] used in our calculation could be workable in the range of less than 450 nm. In order to measure how large the efficiency of the crystal is in the single-pass SHG configuration, we use a relatively strong focus lens (focus length: 5 cm). The measured UV power is 30 μW with 87-mW input pump power at the optimal temperature of 12.5°C. This result gives a conversion efficiency of 0.4% W^{-1}, which is not high compared with other experiments [25–29], the main reason we think may be from the inhomogeneity of the crystal. At the short wavelength, manufacturing the corresponding short period grating is quite difficult. The inhomogeneity of the crystal will reduce the nonlinear coefficient d_{eff} and the conversion efficiency, which have been reported in some experiments [25, 31]. This effect is also observed in our experiment: when we change the incident position of the input laser on the crystal, the power of the SHG changes significantly. Another possible reason is from the short effective length of the crystal. The third possible reason is from the beam quality of the laser. The beam shape of the laser from a diode is elliptical. Although we use a cylindrical lens set to correct the shape of the laser, the beam shape is still not perfect, which also reduces the conversion efficiency. Taking the experimental results, we calculate the effective coefficient d_{eff} to be about 3.3 pm/V according to the Eq. (6) of Ref. [25]; it is quite lower compared with the values obtained in other experiments [25–28].

The schematic drawing of the experimental set-up for SHG in a cavity is shown in Fig. 1. The cw grating-stabilized external cavity diode laser is typically operating with an output power of 100 mW at 780 nm. The frequency of the laser is precisely locked to the cross peak of transition $5\mathrm{S}_{1/2}\mathrm{F} = 2 \rightarrow 5\mathrm{P}_{1/2}\mathrm{F}' = 1, 3$ of Rb^{87} using the saturated absorption technique. Two 36 dB optical isolators are used to cut the reflected light from other optical components. The enhancement cavity is designed in a symmetric bow-tie configuration with a full opening angle of 9°, i. e., 4.5° incident angle on the mirrors. The cavity consists of a flat input coupler M_1 of $T = 2.6\%$ transmission, two high reflecting (HR) mirrors M_3 and M_4 of 80-mm radius of curvature. The mirror M_2 is mounted on a piezo-electric transducer (PZT). The PPKTP is placed in the tight focus between M_3 and M_4; the path length between these two mirrors is about 97 mm. The beam waist inside the cavity is about 37 μm. The total cavity length is about 466 mm. About 57% of the generated UV light transmits though the mirror M_4, which is measured by a power meter. The leak fundamental light through the mirror M_1 and an electro–optical modular (EOM) are used to lock the cavity frequency to the laser frequency by Pound–Drever–Hall method (PDH) [34]. Two lenses are used to make the mode match between the pump mode and the cavity mode. The mode-matched power of the input fundamental light is about 73 mW. The measured finesse of the cavity is about 100. According to these values, we calculate that the circular power of the fundamental light in the cavity is about 1.6 W. We set the temperature of the crystal to be 12.1°C, which is the optimal temperature in the cavity configuration. The reasons that there is a little difference between the phase matching temperatures observed in the single-pass and the cavity configurations are from the following: one is from geometry of the cavity [25]. The input coupler is placed at an angle to the beam axis,

which causes a displacement of the pump beam. This displacement induces a small deviation of the incident angle. Another reason is from our experimental set-up. We put the PPKTP slightly tilted (about 1°) with respect to incident light in order to reduce the feed-back light from the cavity to the diode laser. When the crystal is placed correctly, the strong feed-back light from the cavity easily destroys the locking of our diode laser, even when two 36-dB optical isolators are used. Therefore we have to tilt the crystal to avoid it, which also induces a small deviation of the incident angle. These two effects can be compensated by a change of the crystal temperature. The maximal output power of UV measured is about 3.94 mW. Taking into account the transmission coefficient of the output Mirror M_4 of 57%, the power of generated UV is about 6.9 mW, which corresponds to the net conversion efficiency of 9.5%. The calculated single-pass efficiency in the cavity is about 0.27%/W, which is lower than the efficiency of 0.4%/W observed in the single-pass experiment shown above. The following reasons can be used to explain why the output is quite lower compared with other experiments [25–27]. The first reason has been mentioned previously, which is the lower nonlinear efficient caused by the grating period inhomogeneity of the crystal; another reason is from the small effective length of the crystal. The most dominant reason we think is from the large absorption coefficient of the KTP crystal in blue spectrum region [35] in the range of <400 nm. The measured absorption loss of the crystal is about 27% at 390 nm. Although the circular power in the cavity is not very large, the blue-induced thermal effect should be considered because of this large absorption coefficient. This large absorption makes the stable locking of the cavity difficult, which is shown in the following experimental phenomenon: the developing asymmetry in the cavity transmission signal with corresponding deterioration of the dispersion feature used for stabilizing the cavity, as shown in Fig. 2. Obviously, the fringe of the left in Fig. 2 is broadened because of a self-stabilizing effect of the optical length to laser frequency due to the opto–thermal dynamics where the feedback is positive on this side. Compared with the experiment in Ref. [25], the broadening is quite modest. The scan frequency of the PZT is 24 Hz. We also reduce the scan frequency to 7 Hz to maintain better thermal equilibrium; almost the same phenomenon as shown in Fig. 2 is observed. In order to get a good dispersive signal for stable locking of the cavity, we have to misalign the cavity, which reduces the conversion efficiency and hence the thermal loading of the crystal, as said in Ref. [25]. The misalignment of the cavity likely induces the drop efficiency in the single-pass. During our experiment, we find that the maximal output power can be only kept stable for a few minutes, after that, it drops gradually as time passes. We monitor the output power and find that it is finally kept relatively stable at about 1.7 mW after 4 hours. Besides the blue-induced thermal effect shown above, which makes the temperature of the crystal increased and deviated from the optimal temperature gradually with time, another important reason is the fluctuation of the output laser. The laser used is the external-cavity diode laser with Littrow set-up, small fluctuation of the grating in set-up will cause relatively large position deviation incident on the crystal, which induces a small extra deviation of the incident angle, therefore reducing the output power. Of course, the instability caused from the environment, for example, from air turbulence, dynamic vibration, etc., is also a possible reason. In order to avoid these, we put a box on the cavity, to avoid the possible vibration during the experiment.

We use another same size PPKTP crystal to perform the SHG in the same cavity instead. The maximal measured output power is about 5.08 mW, which corresponds to the generated power of 8.8 mW and the net conversion efficiency of 12%. The same experimental phenomena are observed: the output power drops gradually with time; the cavity transmission signal is also asymmetrical.

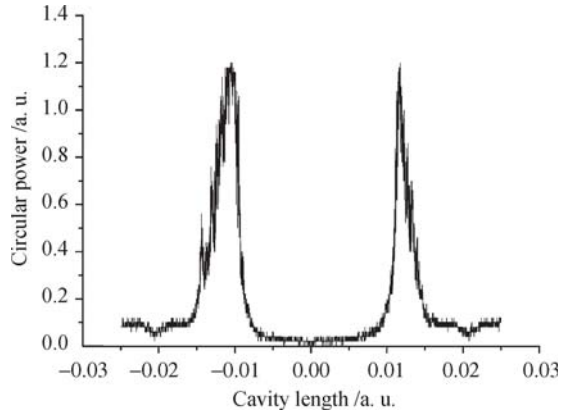

Fig. 2 Pump intensity vs. cavity length change for the two scanning directions of the PZT. The left shows the case of expanding of the PZT and the right shows the case in which the cavity is scanned in the opposite direction.

3 Preparation of the photon pair source in a single-pass configuration

Although the stable output power of cavity SHG is not high, it is enough for us to perform the next experiment. In this section, we will show the preparation of the ultra-bright photon pair source using the output of cavity SHG as the pump laser in a single-pass SPDC configuration.

3.1 Experimental set-up

The experimental set-up is shown in Fig. 3. The violet pump laser with $1/e^2$ diameter of about 2.5 mm used for SPDC is from the doubler shown in the previous section. The output power at 390 nm can be easily adjusted by

changing the input power to the frequency doubler. A lens with 10-cm focal length is used to focus the pump beam. The crystal used for SPDC is another 10-mm long, 1-mm thick and 2-mm wide PPKTP crystal with the periodical poling period of 2.95 μm. The facets of the crystal were also anti-reflection coated at 780 nm and 390 nm. The crystal is mounted in a home-made temperature controlled Peltier oven with the stability of ±0.05°C. After the crystal, a set of lenses consisting of two different focal length lenses (L_2: 38 cm, L_3: 50 cm) is used to couple the photons into a single mode fiber. Before the fiber, two color filters are used to cut 390 nm light. The single mode fiber is connected to a fiber symmetric beamsplitter. Each output of the fiber beamsplitter is connected to a single-photon detector (PerkinElmer SPCM-AQR-14-FC). The outputs of the detectors are sent to a coincidence circuit for coincidence counting, which mainly consists of a variable delay, a coincidence gate and a counting card. The coincidence window is about 5 ns.

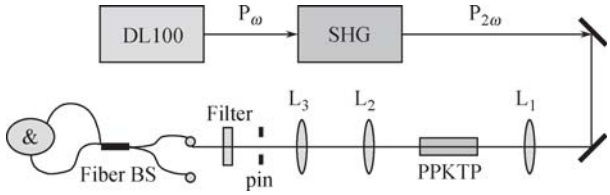

Fig. 3 Schematic set-up. An external-cavity diode (DL100) is frequency doubled in a ring cavity. Output at 390 nm is used as the pump for SPDC. L_1 is a lens with 10 cm focal length, and L_2, L_3 consist of a lens set, their focal lengths are 38 mm and 50 mm respectively. Fiber BS is a fiber beamsplitter.

3.2 Experimental results

The single counts and coincidence counts measured versus the temperatures of the crystal are shown in Fig. 4. The pump power measured before the crystal is about 0.11 mW. The maximal single counts are 2.7 MHz and 2.6 MHz respectively. The maximal coincidence counts are 340 000/s, the optimal temperature of the crystal is about 13.3°C. The coincidence count to single count ratio is about 13%. In order to estimate the accidental single and coincidence counts, a 390-nm half waveplate (HWP) is inserted into the pump beam. The HWP rotates the polarization of the violet pump laser by 90°. In this case, there are no actual SPDC photon pairs. The single counts are from background light, such as the scattered lights from the crystal, mirrors, and the fluorescence related to gray tracking in KTP due to color-center formation. We measure the accidental single and coincidence counts at different phase matching temperatures, and find that they are quite small and almost unchanged with the temperature. Both single counts are less than 50 000/s and coincidence counts are less than 100/s. Therefore, these accidental counts can be safely omitted. The estimated photon pair production rate N

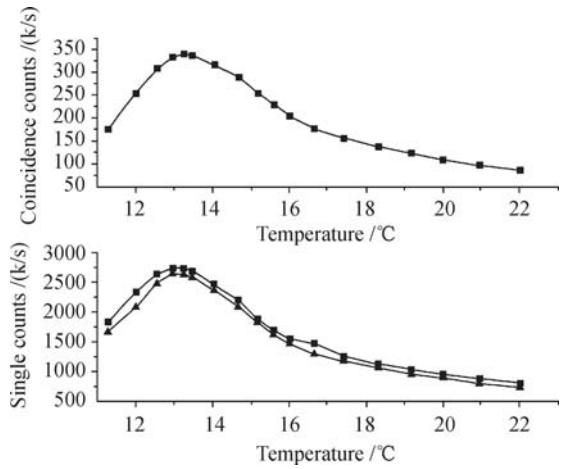

Fig. 4 Single counts (*bottom*) and coincidence counts (*top*) versus the temperature of the PPKTP crystal. No interference filter is used.

can be calculated by the formula $N = \dfrac{S_1 \times S_2}{R_c}$, where, S_1, S_2 are net single counts respectively, R_c is the coincidence count. We calculate that $N = 94 \times 10^6$ Hz per mW pump power. We also measure the single photon spectrum at the temperature of 13.5°C which is close to the optimal temperature by an optical spectrum analyzer (ANDO AQ-6315A with a resolution of 0.05 nm). In order for that, we increase the pump power to about 1 mW. The measured spectrum is shown in Fig. 8 (b). We find that the center wavelengths of idle and signal photons are a little different. The reason will be shown later. The measured bandwidth at FWHM is about 40 nm. Therefore, the production rate is about 2.35 MHz/nm per mW pump power. Furthermore, we insert a 3-nm interference filter in front of the single mode fiber and repeat the measurement shown above. The detected single counts and coincidence counts are shown in Fig. 5. The optimal temperature of the crystal is about 12.44°C. The maximal coincidence counts are about 11 500/s with the pump power of 0.11 mW, corresponding to the production rate of 4.3 MHz/(mW·nm), which is a little higher compared with the production rate without interference filter. We also estimate the accidental single and coincidence counts by the method shown above and find that they are also quite small; both single counts are less than 2000/s and coincidence counts are less than 10/s. One thing we want to point out is that the coincidence count to single count ratio is less than 7%, only half compared with the case of no interference filter inserted. We think one reason is from the fact that the interference filter used is not a perfect square filter and therefore there are photon detection losses associated with the shape of the filter. Another reason is from the fact that there is the transmission loss of the filter even at the center of the filter transmission band, which will reduce this ratio further. We measure that the transmission efficiency of the interference filter at center wavelength is about 90%.

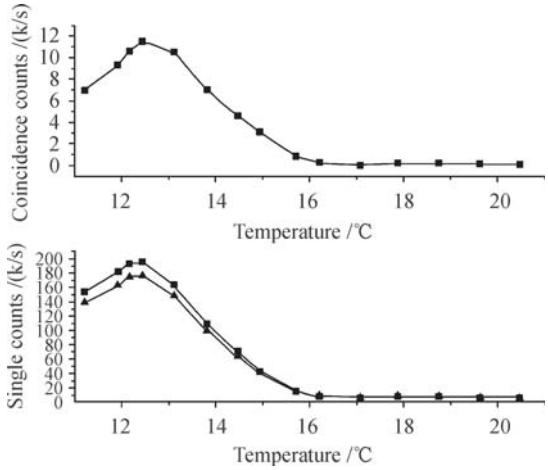

Fig. 5 Single counts (*bottom*) and coincidence counts (*top*) versus the temperature of the PPKTP crystal. A 3-nm interference filter is used.

3.3 Discussion

One thing we want to address is that the measured temperature bandwidth in our SHG experiment with PPKTP is about 2.6 K. However, from Fig. 4, we can see that the measured temperature bandwidth is much larger than the 2.6 K with the same crystal. (We only get half of the temperature spectrum experimentally in order to avoid the possible liquefaction on the surface of the crystal at lower temperature. Suppose the temperature spectrum is symmetric.) This is easy to be understood from the following fact: the band of the SHG is measured with the wavelength of both pump components being equal at all times. On the contrary, the single and idle photons in SPDC can vary in opposite directions when the temperature is changed. This difference makes the SPDC have a more broad temperature band. Our simple calculation confirms this point.

From Fig. 4, we can see that single and coincidence counts depend significantly on the phase matching temperatures of the crystal. One more thing is that even the temperature of the PPKTP is shifted away from the optimal temperature quite significantly, for example almost 10 degrees, still we detect very high coincidence counts and the coincidence count to single count ratio is more than 10%. We think there are three possible reasons: one is due to the spatial mode variation of the SPDC outputs and the subsequent coupling into the single mode fiber. It is well known that the SPDC output is a beam-like solid cone for the collinear operation, and becomes a wide-open cone if the phase matched temperature is detuned from the optimal temperature. The coupling of the SPDC output to the single mode fiber is optimal for the beam-like solid cone but is substantially reduced for a wide-open cone, this case will reduce the single counts and coincidence counts. In order to check this possible reason, we calculate the angles of the open cones of SPDC outputs versus the temperatures of the

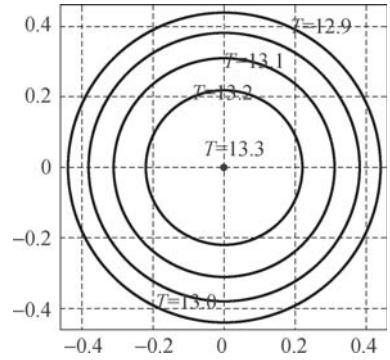

Fig. 6 The calculated emitted angles of SPDC outputs at different phase matching temperatures in degenerated case. Unit of temperature T: °C; unit of angle: (°).

crystal in degenerated phase matched cases. The results are shown in Fig. 6. The results show that at the optimal temperature and the output of the SPDC is a solid cone, the angle of SPDC output increases with the decrease of the temperature. When the temperature is higher than the optimal temperature, there is no output of SPDC, which is in contradiction with the experimental results. Therefore, we conclude that this spatial mode variation of the SPDC outputs may have an effect on the single and coincidence counts only at lower temperatures. Another possible reason is due to the nondegenerated phase matching SPDC of the crystal at different temperatures. We demonstrate this effect by the following two facts: one is that we calculate the wavelengths of the SPDC outputs versus the temperatures of the crystal in collinear non-degenerated phase matched case, and the results are shown in Fig. 7. We clearly see that the wavelengths of the SPDC outputs change with the temperatures of the crystal. Another fact is from our measured single photon spectra at different temperatures. From these spectra, we clearly see that the center wavelengths of two photons become different with the temperatures, and the bandwidth of single photon becomes narrower, which are

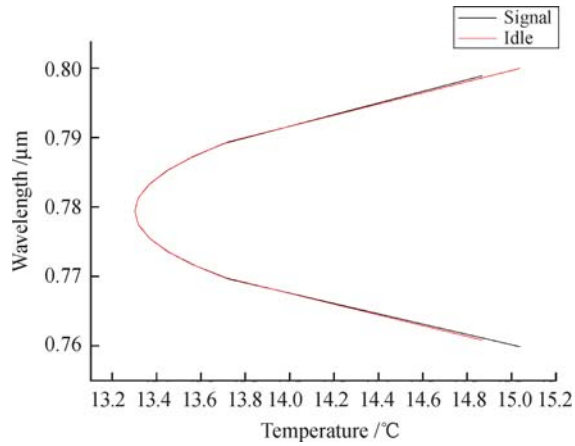

Fig. 7 The wavelengths of the SPDC outputs versus the temperatures of the crystal in collinear non-degenerated phase matching case.

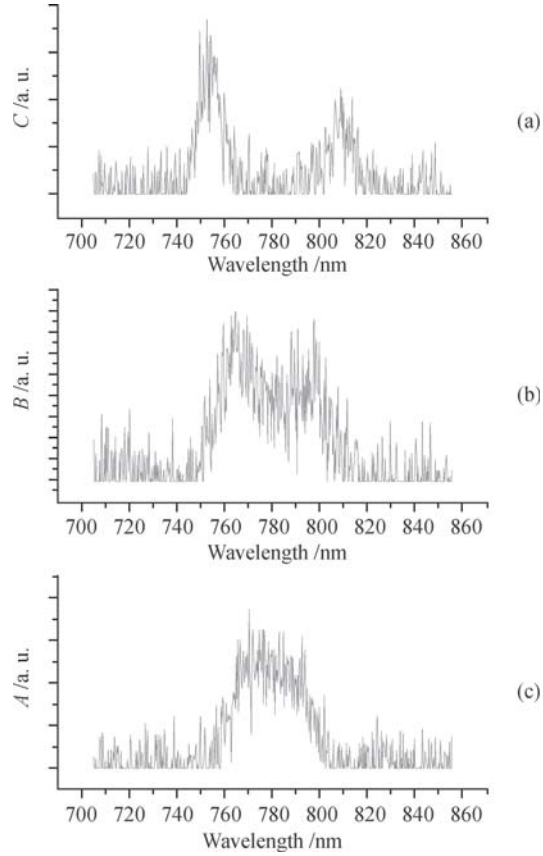

Fig. 8 The measured single photon spectrums at different temperatures of the crystal. The pump power is about 1 mW. **(a)** $T = 12.23°C$; **(b)** $T = 13.50°C$; **(c)** $T = 16.56°C$. y-axis stands for the intensity (a.u.).

shown in Fig. 8. The third possible reason is from the inhomogeneity of the crystal, which also induces the non-degenerated phase matched SPDC. We also calculate the wavelengths of the SPDC outputs versus the periods of the PPKTP grating in collinear phase matching case. The results are shown in Fig. 9, which clearly shows that the inhomogeneity of the crystal will induce the non-degenerated phase matching SPDC outputs. We think these three effects may also explain the reason why the optimal temperature in the case of a 3-nm interference filter inserted is different from the case without filter.

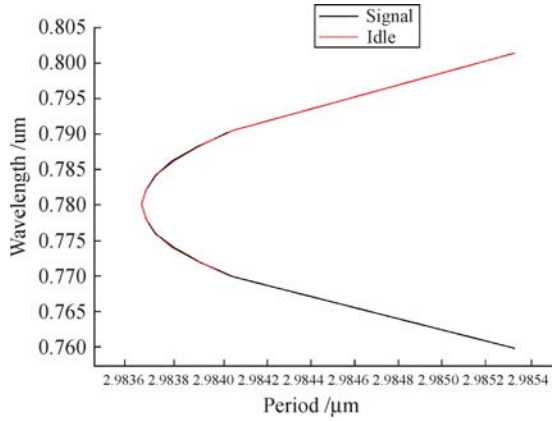

Fig. 9 Wavelengths of the SPDC outputs versus the periods of the grating in collinear phase matching case.

According to the measured optimal temperature of 13.3°C, we can calculate the period of the grating, which is about 2.98 μm, a little larger than the 2.95 μm given by the manufacturer. This may be due to the imperfections in the poling process. Because the dispersion increases rapidly in the UV region, the quasi-phase-matching (QPM) condition requires short domain-inversion grating (< 4 μm). It is not easy to fabricate such short QPM grating homogeneously.

We think the main reasons that our photon pair source is highly efficient are from two facts: one is we use the type-I phase matched PPKTP crystal. As we show, the highest d_{33} nonlinearity of KTP is used in the type-I case, instead of a relatively small d_{24} nonlinearity in the type-II case; another is we use a set of lenses to couple output of SPDC to a fiber, which helps us to realize the optimal coupling of the SPDC outputs to the single mode fiber. Although there are many experiments that report the highly efficient generation of photon pairs [30, 36–44], there are few experiments in which a bulk type-I phase matched periodical poled crystal is used. Furthermore, most experiments are focused on the preparation of the entangled photon pairs with the aid of some techniques [38, 40–42], therefore it is not suitable to compare our result with them. In Ref. [43], more than 7400/s coincidence counts in a type-I phase matched bulk PPKTP with the input power of 3.58 mW is reported. The production rate was about 0.73 MHz/mW with full bandwidth, which is lower than in this work. In Ref. [44], a bulk type-II phase matched PPKTP is used to generate a photon pair, the detected photon pairs are 24 000/(s·nm) with the injected pump power of 0.81 mW, corresponding to the production rate of 1.0 MHz/(nm·mW). Our result is higher than that. Besides, there are some reported experiments in which a photon pair is generated in a PPLN waveguide. For example, Ref. [36] reports detected photon pairs of 1550/s for a 5.2 μW of input pump power in 30-nm bandwidth in a type-I phase matched PPLN waveguide, corresponding to the production rate of 48 MHz/(mW·nm). Ref. [44] reports a detected coincidence counts of 35 000/(s·nm) with the input power of 33 μW in a type-II PPKTP waveguide, corresponding to about 25-MHz/(nm·mW) production rate. Both are higher than our results. This is because usually the waveguide is more efficient than the bulk crystal, the main reasons are already shown in Ref. [44].

4 Generating a multi-mode photon pair with the aid of cavity

From the results shown in the previous section we see that although an ultra-bright two-photon source can be obtained with the aid of a periodical poled nonlinear crystal, the bandwidth of the photon is very broad, which

makes the direct coupling between the photon and the atom impossible. Therefore the bandwidth of the photon has to be reduced significantly, which can be realized by putting the down-converter crystal in a cavity. In this way, only the photon whose frequency matches the cavity mode will be enhanced significantly. In this section, we report on the generation of a type-I multimode two-photon state on a rubidium D_2 line (780 nm) using PPKTP crystal with the optical parametric oscillator (OPO) operated far below threshold and observation of an oscillatory correlation function. The theory of the output from an OPO far below threshold has been discussed in Refs. [15, 19], so here we mainly focus on the experimental results discussion.

A schematic drawing of the experiment set-up is shown in Fig. 10. The pump laser is still from our doubler introduced previously. The OPO cavity is composed of two concave mirrors of curvature radius 80 mm and two plane ones. The concave mirror (M_3) has partial transmission about 5% at 780 nm and works as the output coupler, while the others are high reflectance mirrors. The round-trip length of the cavity is 480 mm corresponding to 0.625 GHz FSR and 1.6 ns round-trip time. The distance between two spherical mirrors is about 100 mm, and a 10 mm long PPKTP is placed between two spherical mirrors resulting in a waist of 40 μm inside the crystal. The temperature of the crystal is controlled by our home-made thermoelectric cooler. The OPO cavity is locked to laser frequency by PDH method. The triangle cavity C is used to get mode-matching between two bow-tie-type ring cavities. It is very important to have a good mode matching between these two cavities, because it can increase the pump efficiency and inhibit the excitation of the complicated transverse spatial modes of the OPO. The mode match is done by matching both the harmonic pump laser from the frequency doubler and the harmonic field from OPO cavity to the triangle cavity C. To get the second harmonic field from the OPO cavity,

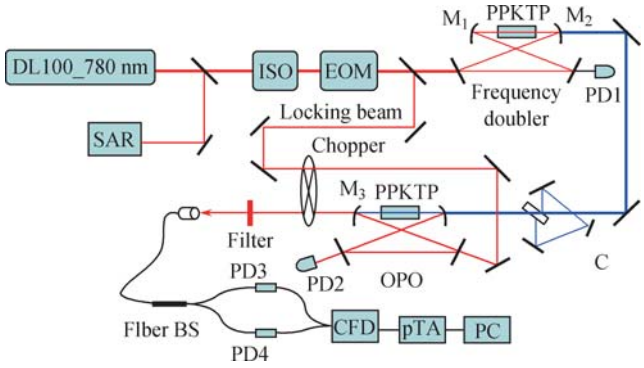

Fig. 10 Experiment set-up. DL100_780 nm: ECDL operated at 780 nm; ISO: optical isolator; EOM: electro–optic modulator; SAR: saturated absorption resonator; PD1 and PD2: fast photodetector for cavity locking; PD3 and PD4: avalanche photodetectors; CFD: constant-fraction discriminator; pTA: picosecond time analyzer.

we input a reference light that is a part of the fundamental laser to OPO cavity for frequency doubling. A chopper is used to cut the photons of locking light reflected from the surface of the crystal to avoid possible background noise, because the locking beam has the same frequency and polarization as the generated photon pairs. The colored glass filer is used to cut the UV light. The outputs from OPO are coupled into a 50/50 fiber beam-splitter (BS). The outputs of the BS are input to single photon detectors. The outputs of the detectors are sent to a coincident circuit for coincidence counting, which mainly consist of a picosecond time analyzer (ORTEC, pTA9308) and a computer.

In order to generate a two-photon state, the OPO should operate far below its threshold. This threshold can be calculated by the formula: $p_{\rm thr} = \dfrac{(T+L)^2}{4E_{\rm nl}}$, where, T is the transmission of the output coupler, L is the loss in the cavity. $E_{\rm nl}$ is the nonlinear coefficient of the crystal. Taking the measured nonlinear coefficient shown in Section II, and omitting the loss in the cavity, the calculated threshold is about 160 mW. In our experiment, the input power is about 15 μW, which is far below the threshold. Figure 11 shows the measured intensity cross-correlation function between the generated photons in the experiment. The points are the measured data, and the line is the fitted curve using Eq. (5) of Ref. [19]. The theoretical curve fits the experiment data quite well.

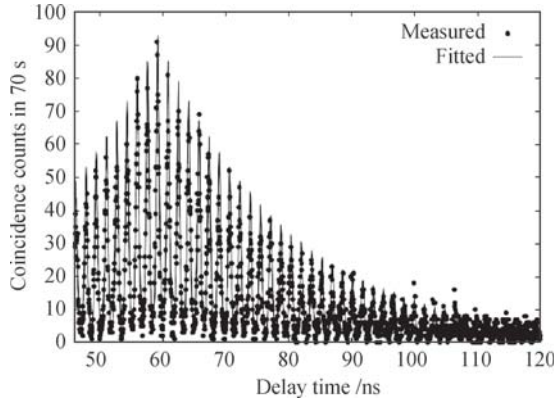

Fig. 11 Observed oscillatory correlation function of multimode two-photon pairs. The points are the measured data, and the line is the fitted curve using Eq. (5) of Ref. [19]. The coincidence counts are accumulated in 70 seconds. The pump power is about 15 μW. The fitted parameters of curve line are as follows: $C_1 = 93, C_2 = 0, \Delta\Omega_{\rm OPO}/(2\pi) = 7.8$ MHz, $\tau_0 = 59$ ns, $\tau_{\rm OPO} = 1.63$ ns, $\tau_D = 220$ ps.

This is, to our best knowledge, the first time that this kind of oscillatory correlation function at Rb D_2 line has been obtained. Cross-correlation between two photons shows a cavity bandwidth of 7.8 MHz. Besides, our experiment is different from others. In Ref. [15], a bigger and more expensive Ti:Sapphire laser is used as the fundamental light for the SHG in a cavity. Our fundamental

source is a small and relatively cheap grating-stabilized external cavity diode laser and its frequency is locked to the transition line D_2 of Rb^{87} atom by the saturated absorption technique. In Ref. [16], a pair of cw type-I down converters, one rotated by 90°, in a ring cavity is used to produce polarization-entangled photons. In this experiment, a Ti:Sapphire laser and a $KbNO_3$ crystal are used. In our experiment, a PPKTP crystal, which has larger nonlinear coefficient, is used to compensate the relative lower power of the diode laser. In Ref. [17], a cw type-II down converter is used to get a narrow-band photon pair at 795 nm with an ECDL at 397.5 nm. In our experiment, the pump laser at 390 nm for OPO is from frequency doubling of the 780-nm laser in a cavity. In Ref. [18], a single resonant OPO is used to prepare a narrow-band photon. The OPO is locked by Hansch–Couillaud method.

In this experiment, we obtained a multi-mode photon pair with the aid of a cavity. A question arises very naturally: what is the difference between these photons and the photons generated in a single-pass SPDC configuration? In the next section, we will show some special properties by using a two-photon interference experiment.

5 Quantum interference of multi-mode two-photon pairs with a Michelson interferometer

Goto *et al.* [45] recently reported on the second-order interference of multimode two-photon pairs with an unbalanced Mach–Zehnder interferometer. They theoretically showed that the second-order time correlation between the two photons has a multipeak structure, and its shape depends on the path length difference between two interfering beams. But in their experiment, they only consider a case in which the propagation time difference between short and long paths in the interferometer is half of the round-trip time of the photon in the OPO cavity. This makes their theoretical claim lack enough experimental support. In order to further investigate the properties of the multimode photon pairs, we perform a quantum interference experiment in a Michelson interferometer in more general cases. We not only discuss the case in which the interferometer is highly unbalanced, considered in Ref. [45], but also discuss the case in which the interferometer is nearly balanced, which is not included in Ref. [45], extending the discussions of Ref. [45]. The results obtained by Goto *et al.* and ours clearly show the different interference behavior of multimode photon pairs from the photon pairs obtained through a single-pass SPDC configuration. We believe these results are useful to further characterize the properties of the photon pairs obtained via an OPO far below threshold. The detailed theory discussion can be found in Ref. [23]. Here, we only discuss the experimental results.

A schematic drawing of the experimental setup is shown in Fig. 12. The outputs from OPO cavity are inputted into a Michelson interferometer. The photon generated has a comb-like shape of the spectrum shown in Section 4. The phase difference between two interfering beams can be adjusted by moving the position of the mirror M_1, which is mounted on a piezoelectric transducer (PZT). Both PZT and the mirror are fixed on a translation stage, by which the path length difference can be roughly adjusted. The relative phase between two interfering beams can be actively controlled and locked by PDH method. One output of the interferometer is connected to a 50/50 fiber beamsplitter (BS) (NEWPORT P22s780BB50). Each output of the fiber BS is connected to an avalanche photon detector. The outputs from detectors are sent to a coincidence circuit for coincidence counting, which mainly consists of a picosecond time analyzer and a computer.

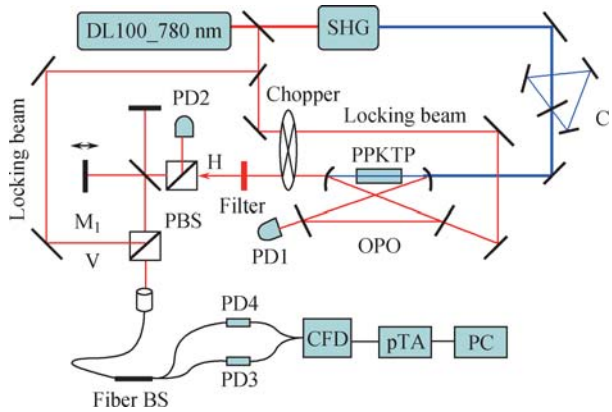

Fig. 12 Schematic of the experimental set-up. DL100_780 nm: diode laser; PBS: polarization beam splitter; PD1 and PD2: photodetectors for locking; PD3 and PD4: avalanche photodetectors; Fiber BS: fiber beamsplitter; C: triangle cavity; pTA: picosecond time analyzer; H: horizontal polarization of the locking beam; V: vertical polarization of the OPO beam; CFD: constant-fraction discriminator.

First, we show our experimental results in the unbalanced case, where the path length difference between two interfering beams is about 170 mm, equal to about 1/3 of the round-trip length. In this case, photons propagations in the interferometer can be divided into two different situations. In situation 1, both photons are reflected or transmitted at the BS of the interferometer, which will provide the second-order interference; in situation 2, one of the two photons in each pair is reflected and the other is transmitted there, there is no second-order interference. In both situations, there is no first-order interference because the path length difference is much larger than the first-order coherence length of the single photon. The experimental results are shown in Fig. 13. The dots are experimental data, and the lines are fitted by the Eq. (4) of Ref. [23]. The experimental results show that the second-order time correlation has a multi-

peak structure. The shape of the fringe is different from that shown in Ref. [45]. This concludes that time correlation is really dependent on the path length difference. Our results clearly support the theoretical claim given by Goto *et al.*. In Fig. 13, the deviation of the experimental data from the fitted lines is probably due to the small round-trip time, which determines the distance between adjacent peaks. If round-trip time is larger, every peak could be more distinguished from neighbors even under the condition of the bad resolving time of the detectors. A better agreement between the data and fitted lines could be achieved.

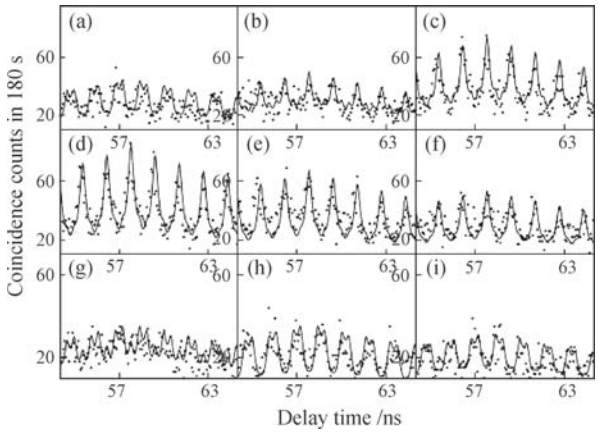

Fig. 13 Experimental results in highly unbalanced case. The dots are experimental data, and the lines are fitted by the Eq. (4) of the Ref. [23]. The experimental results show that the second-order time correlation has a multipeak structure. The phase θ increases stepwise by arccos $j/4$ from **(a)** to **(i)** ($j = -4, -3, \ldots, 4$).

Next, we extend the experiment to the case in which the two interfering beams in the interferometer are nearly balanced. We divide this case into two different situations according to the first-order coherence length of the single photon (about 90 μm [24]): in situation 1, two interfering beams are perfectly balanced, where the path difference is almost zero. There are two different interferences in this situation: one is the second-order interference, which is caused by the superposition of the terms: the term both photons are reflected or the term both photons are transmitted at the BS, this provides a phase sensitive interference, and the term one of the two photons in each pair is reflected and the term the other is transmitted at the BS of the interferometer, which provides a phase insensitive Hong–Ou–Mandel [46] interference; another is the first-order interference, which is caused by the superposition of two probabilities: the probability one photon is reflected or the probability this photon is transmitted at the BS; this is a phase sensitive interference. In situation 2, two interfering beams are almost balanced, but the path length difference between two interfering beams is slightly larger than the first-order coherence length of the single photon. Therefore, there is no first-order interference besides the second-order interference caused by the superposition of the terms: the term both photons are reflected or the term both photons are transmitted at the BS. The experiment results are shown in Fig. 14. Figure 14 (a)–(c) indicates the time correlation functions in situation 1, where θ=0 and π correspond to the maximum and minimum heights of the correlation functions. Figure 14 (d) shows the result in situation 2, where path difference is 0.74 mm, and θ is arbitrary phase. The experimental results clearly show that the second-order time correlation has a multipeak

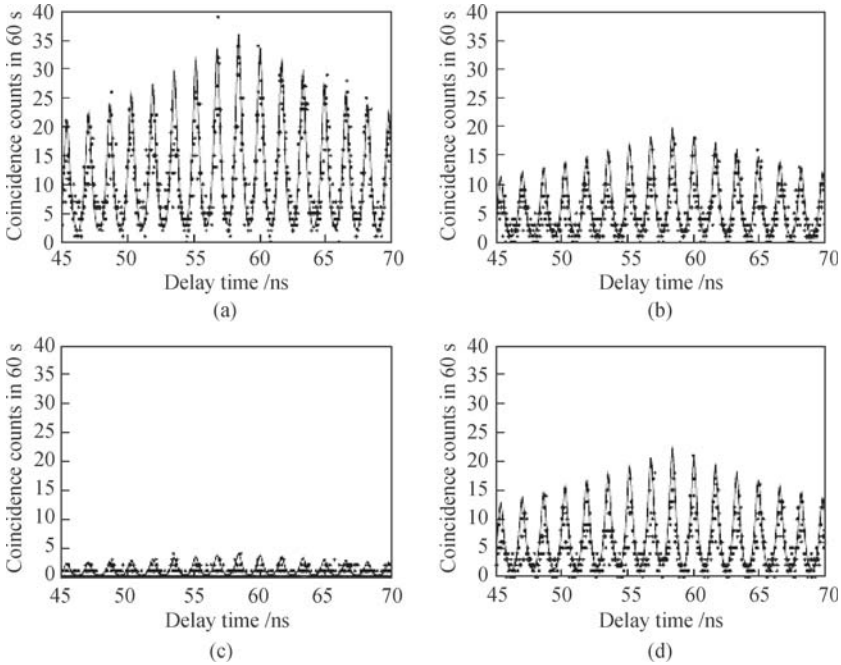

Fig. 14 The time correlation functions of the two-photon interference in balanced case are measured. **(a)** to **(c)** corresponds to $\theta = 0, \pi/2, \pi$ respectively in situation 1. **(d)** is measured at an arbitrary phase in situation 2 with $\Delta L = 0.74$ mm for comparison.

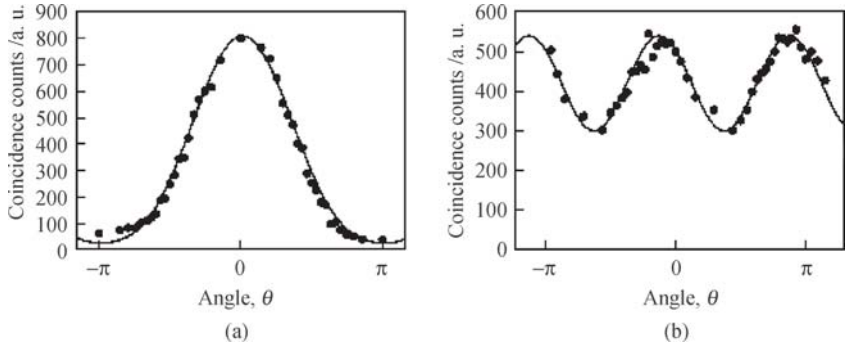

Fig. 15 **(a)** and **(b)** are the coincidence counts of the two-photon interference in case of $\Delta L \approx 0$ and $\Delta L = 0.74$ mm, respectively.

structure, but it is very different from that in the unbalanced situation. The shapes of four pictures in Fig. 14 are almost the same except for their heights. We see that the shape of the correlation function is independent of the small path length difference between two interfering beams. This can be easily understood from Eqs. (6) and (7) of Ref. [23]: the shape of the correlation function is independent of the phase. Therefore, our experimental results agree well with the theoretical predictions. The height of Fig. 14(c) is not exactly zero, which is because of the phase fluctuation as well as the imperfection of the 50/50 beamsplitter in the interferometer. In addition, we measure the coincident counts against the phase differences between two interfering beams. Figure 15 (a) and (b) shows the results in situations 1 and 2 respectively. The visibility of Fig. 15 (a) is about 88% against the perfect case of 100% and the visibility of Fig. 15 (b) is about 29% against the perfect case of 50%. The possible reasons of the lower visibility are as follows: the shift of the light from ECDL during the experiment; the small shift of the mirror positions; the phase fluctuation and so on. Comparing Fig. 15 (a) and (b), we see that the peaks have a spacing in situation 1 that is twice as long as the peaks spacing in situation 2, which agrees with the theoretical predictions of Eqs. (6) and (7) of Ref. [23].

In this section, we clearly show some special properties by using a Michelson interferometer. The results show the different interference behavior of the multi-mode photon pairs from the photon pairs generated through a single-pass SPDC configuration. Another important thing we want to know is how long the coherence length of the photon is. The answer to this question is very important because a long coherence length means a narrow bandwidth of the photon and possible strong coupling between the photon and the atomic system, and this efficient coupling is the prerequisite for realizing an atomic-based quantum network. Long coherence length of the single photon is also a key point in many quantum protocols, such as quantum teleportation [47], swapping [48], and so on. This motivates us to experimentally evaluate the coherence length of the single photon generated. In the next section, we will show the experiment measuring the coherence length of the photon.

6 Experiment measuring the coherence length of the single multi-mode photon

The basic idea of this work is as follows: when a photon is inputted to a Michelson interferometer, if the path difference between two interfering beams is larger than the coherence length of the photon, there is no first-order interference. If the path difference is less than the coherence length of the photon, then there is a first-order interference and the single count rate depends on the fine path difference of the order of the single photon wavelength; the maximal 100% interference visibility could be observed in the ideal case. Based on this idea, we divided our measurement on the coherence length of the single photon into two steps. In the first step, we try to estimate the range of the interference observed by coarsely changing the path difference between two interfering beams. In the second step, we try to get the oscillation of the single count rate by finely adjusting the path difference.

The schematic drawing of the experimental set-up is shown in Fig. 16. The input power of UV light at 390 nm to OPO is only 50 μW. A two-photon pair is generated through the OPO. The outputs from OPO are inputted into a Michelson interferometer. The path difference between two interfering beams can be adjusted by moving the mirror M_1 mounted on a PZT. Both PZT and mirror are mounted on a translation stage. The relative phase between two interfering beams can be actively controlled. One output of the interferometer is connected to a single mode fiber, then sent to a single photon detector. The output of the detector is sent to a computer for counting. The count time is 1 s.

First we coarsely change the path difference between two interfering beams by moving the translation stage to estimate the range of the interference we can observe. Figure 17 shows the single counts against the path differences between two interfering beams. The squares show

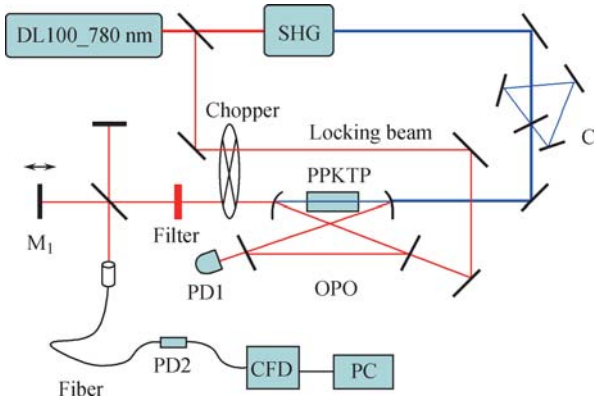

Fig. 16 Experimental set-up. DL100_780 nm: an external-cavity diode laser operated at 780 nm; SHG: second harmonic generation; OPO: degenerated optical parametric oscillator; C: triangle cavity for mode-matching; M_1: mirror mounted on a PZT and a translation stage; PD1: fast photodetector for cavity locking; PD2: single photon detector; Filter: red color glass; CFD: constant-fraction discriminator.

the experimental data when the two interfering beams are in phase, the upper curve (*online black line*) is fitted by the function of $A\sin c^2[C(x-B)]+D$. The dots are the experimental data when the phase difference of the two interfering beams is π, the down curve (*online red line*) is fitted by the function of $-A\sin c^2[C(x-B)]+D$. Where, A, B, C and D are fitted parameters, and are 24, 6.565, 35 and 44, respectively. From this figure, we can see that when the two interfering beams are almost equal, there is a first-order interference pattern. When the path difference is large, there is no first-order interference. The range at FWHM of the interference profile is about 90 μm, this corresponds to about 3 nm bandwidth assuming the single photon have a *Gaussian* wave packet. Then we make the two interfering beams of the Michelson interferometer almost perfectly balanced, and finely adjust the path difference by PZT to observe the oscillation of the single count rate against the phase. The experimental results are shown in Fig. 18, which clearly shows that the single count rate oscillates with the phase. The visibility is about 65%. The little lower visibility is mainly due to the imperfection of the interferometer. Our experimental setup is aligned by an ancillary light. The single photon from OPO cavity may not overlap with this ancillary light perfectly in the interferometer. Therefore the interferometer is aligned perfectly for the ancillary light, but is not aligned optimally for the single photon from SPDC. The main contribution to the large error bars in Fig. 17 is from the side peaks. The fitting lines agree very well with the center peaks, but deviate from the side peaks obviously. The reason is not clear, but we guess that it is still from the imperfection of the interferometer and possible phase fluctuation between two interfering beams. In side peaks, the interference visibility is quite lower, and a small fluctuation of data will cause a quite large deviation from the fitting line. We check and find that the background noise from light scattering of other optical components, such as mirrors, is quite small and therefore can be omitted.

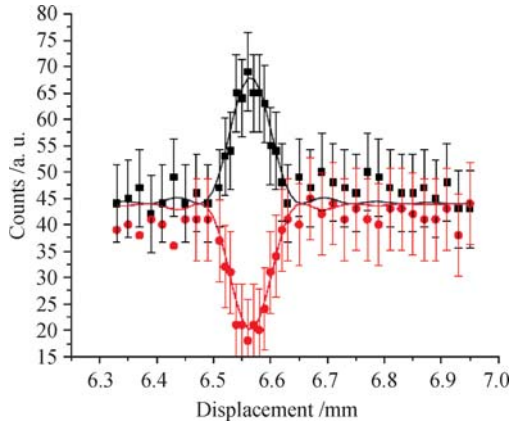

Fig. 17 The single counts against the path differences between two interfering beams. The dots and squares are experimental data and the solid lines are the fitted lines by $\sin c^2$ functions.

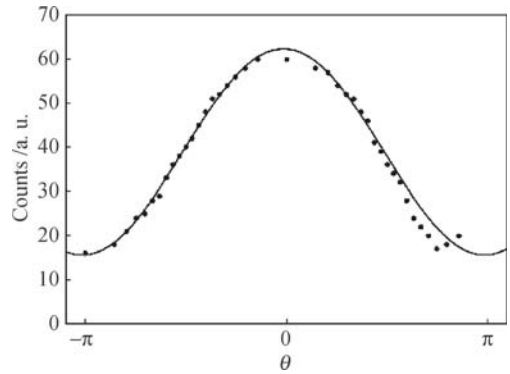

Fig. 18 The single counts against the relative phases between interfering beams when Michelson interferometer is in perfect balance. The dots are experimental data and solid line is the fitted line by cos function.

Compared with the about 40 nm spectrum at FWHM of the single photon generated in a single pass SPDC configuration [9], the bandwidth of the single photon is reduced significantly. Following the treatment given by Ou [49], we now do a raw estimation on the coherence length of the single photon. In our experiment, a type-I phase matched down-converter is used. There are a number of non-degenerated conjugate modes separated by the free spectral range (FSR) of the OPO cavity. These mode pairs are located in the spectrum on the two sides of degenerated mode pair. Assume there are m pairs non-degenerated modes, the bandwidth of the output of the OPO is $2m\times\Delta\Omega_{\rm OPO}$, where $\Delta\Omega_{\rm OPO}$ is the FSR of the OPO cavity, $m\approx(l+n_0d+n'\omega_0d)\Delta\Omega_{\rm OPO}/(2\pi c)$, where, l is the cavity length excluding the crystal, d is the length of the crystal, n is the index of refraction of the crystal, $n'=\partial n/\partial\omega$ [49]. Taking into account our experimental parameters of l=47 mm, d =1 mm, $\Delta\Omega_{\rm OPO}=2\pi\times0.625$ GHz, we calculate that $m=964$, therefore the bandwidth of the single photon is about 1205 GHz. Assuming that the photon have a *Gaussian* wave packet, then the estimated coherence time is about

360 fs, and the coherence length is about 110 μm, which is close to the measured 90 μm coherence length in the experiment.

From the discussion shown above, we see that even the photon is generated through the OPO far below threshold. The bandwidth is still so large that the direct coupling between the photon and the atom is impossible, therefore a further reduction on the bandwidth is necessary. In the next section, we will show how to reduce the bandwidth of the photon.

7 The generation of a narrow-band photon pair

As we know, because of the large bandwidth of SPDC photons, there are numerous non-degenerate conjugate pairs together with degenerate pairs. The non-degenerate pairs are located at two sides of the degenerate frequency of OPO (ω_0) with a spacing of $\Delta\omega_{\rm FSR}$, the FSR of the OPO cavity, and have about the same strength as the degenerate one. Therefore, a passive filter is needed to eliminate these non-degenerate modes. This can be done by using a filtering cavity that has a bandwidth larger than that of single mode down-conversion [15].

The schematic drawing of the experimental set-up is shown in Fig. 19. The pump laser is still from the output of the doubler. Different from the experimental setup in Ref. [19], the OPO cavity is composed of a plane mirror and a concave mirror of curvature radius 35 mm. The concave mirror and the plane mirror have partial transmissions of about 0.5% and 1.1% respectively at 780 nm wavelength. The PPKTP crystal is placed between the plane and concave mirrors. The cavity length of the OPO is about 25 mm, the FSR is about 6 GHz. The measured finesse of OPO is about 250, which is higher than that of the bow-tie-type cavity used in Ref. [19]. The higher finesse means higher photon flux [15]. The OPO cavity size is much smaller than that in Ref. [19], and the smaller size makes better stabilization of the system possible. The temperature of the crystal is also controlled by a home-made thermoelectric cooler with a stability of 0.02°C. The FSR of the filter cavity is about 30 GHz. The measured finesse is about 100. The selected single-mode outputs from the filter cavity are inputted to a 50/50 beam-splitter. The outputs of the BS are coupled to single mode filters which are connected to single photon detectors. The detector works in gate mode in order to reduce the background noise caused by locking light further. The outputs of the detectors are sent to a coincident circuit for coincidence counting, which mainly consist of a counting card (FAST ComTec P7888-2) with 1 ns bin width and a computer. In order to make the SHG cavity and OPO more stable, these two cavities are kept under two boxes in order to avoid influence from the environment.

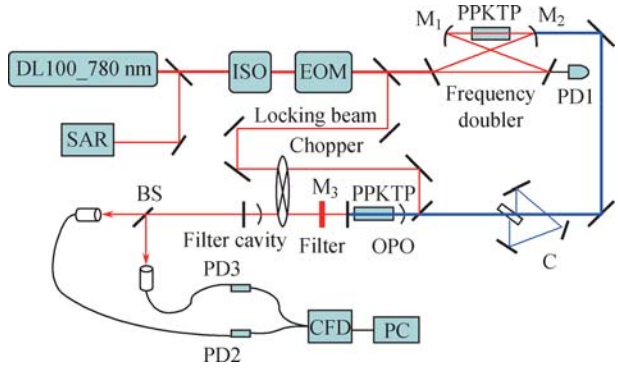

Fig. 19 Experimental set-up. DL100_780 nm: ECDL operated at 780 nm; ISO: optical isolator; EOM: electro–optic modulator; SAR: saturated absorption resonator; PD1: fast photodetector for cavity locking; PD2 and PD3: avalanche photodetectors; CFD: constant-fraction discriminator; C: triangle cavity; BS: beam splitter; M: mirror.

Figure 20 shows the measured intensity cross correlation between two photons. The dots are measured data, and the solid line is a fitted line by the function of $\exp(-\Delta\omega_{\rm OPO}\,|\tau-\tau_0|)$, where, $\Delta\omega_{\rm OPO}$ is the bandwidth of the OPO, τ_0 is the electronic delay. As can be seen from Fig. 20, the fit agrees very well with the experimental data. The small misfit may come from the modification from the spectrum of the SPDC by the filtering cavity [15]. According to the fitted line, the estimated bandwidth of the photon is about 21 MHz, which is comparable to the natural linewidth of Rb atom.

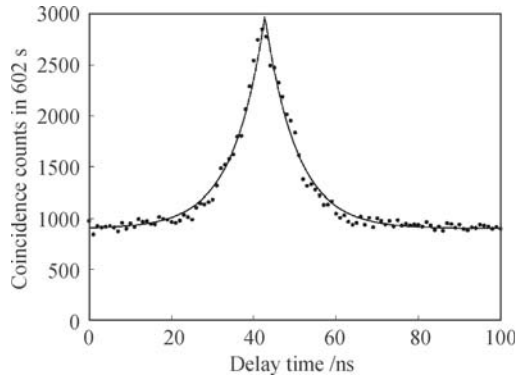

Fig. 20 The measured intensity cross correlation function between photons. The pump power input to OPO is about 1.08 mW. The dots are measured data, and solid line is fitted line by the function $\exp(-\Delta\omega_{\rm OPO}\,|\tau-\tau_0|)$. $\Delta\omega_{\rm OPO}$=21 MHz, and τ_0 is the electronic delay. The accumulated time is 602 s.

Besides our work [20], there have been some other progresses along this research direction recently [15, 50, 51]. Our experiment is different from those experiments: in Ref. [15], a bigger and more expensive Ti:Sapphire laser was used as the fundamental light for the second harmonic generation (SHG) in a cavity. Our fundamental source is a small and relatively cheap grating-stabilized external cavity diode laser, and laser frequency is precisely locked to the transition line D_2 of Rb^{87} atom by

the saturated absorption technique. In Ref. [50], a cw type-II down converter is used to get a narrow-band photon pair at 780 nm. In that experiment, the pump laser used for SHG at 390 nm is a Ti:Sapphire laser. An etalon is used to select the single-mode photon pair from the output of the OPO. In our experiment, the pump laser for SHG is from ECDL. The nonlinear crystal is type-I phase-matched. A spectral filtering cavity, whose resonant frequency is locked to the fundamental laser, is used to select a single-mode photon pair from the OPO output. The use of a diode pump laser is an important step towards the miniaturization and simplification of the system. In Ref. [51], two type-II phase matched PPKTP crystals are used, one is for down-converter, the other is for compensation crystal, by which, both signal and idle photons which have orthogonal polarization directions can be made resonant to the cavity. The wavelength of the photon is 894.3 nm, which corresponds to cesium D_1 line. Our work is the first work with a type-I phase matching crystal at 780-nm wavelength and a diode laser system.

The further reduction of the bandwidth of the photon can be achieved, for example, by improving the finesse of the OPO cavity. The finesse of the OPO cavity is inversely proportional to the sum of the coupling constants of the mirrors and the transmission loss of the light through crystal. The limitation on the finesse of OPO cavity is mainly from the transmission loss that the photon transmits through the PPKTP crystal, which is determined by the property of KTP crystal. It should be pointed out that achievable bandwidth of the photon is no less than 1 MHz even with the more high finesse cavity, because the bandwidth of the diode laser we used is about 1 MHz. During the experiment, the pump power input to the OPO is about 1.08 mW. The detected rate of the single-mode photon pair is about 50/(s·mW), corresponding to 2.7/(s·MHz·mW). Taking into account the loss from the 50%–50% beam-splitter used, the detectable rate is about 5.4/(s·MHz·mW). The result is higher than the detected pairs rate of about 0.2/(s·MHz·mW) using passive filtering [52], in which, a single-pass SPDC configuration is used. The result is comparable to the result shown in Ref. [50], in which, a photon with 9.6 MHz bandwidth is generated with the detected photon pair rate of 6/(s·MHz·mW). One more thing we want to point out is that a type-I phase-matched PPKTP crystal is used as the down-conversion crystal in this work. As we know, the highest d_{33} nonlinearity of KTP is used in the type-I case, instead of the relatively small d_{24} nonlinearity in the type-II case; therefore, we should obtain a higher photon pair rate compared with that in Ref. [50]. However, the problem is that the bandwidth of the photon generated in type-I phase-matched configuration is much larger than that of the photon generated in type-II phase-matched configuration [49]. Therefore, there are much more multi-modes in OPO cavity in the type-I case compared with that in the type-II case under the same configuration, this is the reason why our photon pair rate per mode is comparable to the result shown in Ref. [50]. The further improvement of photon pair rate could be achieved for example, via the OPO cavity with higher finesse. In Ref. [15], it has been shown that the average enhancement factor per mode with OPO cavity compared with signal rate without OPO cavity is roughly the square of the number of finesse. It was shown in Ref. [50] that the pair generation rate is proportional to the pump power. Of course, the increase of input power can enhance the detected photon pairs, but the number of multiple photon pair is also increased, which will introduce the large background noise and reduce the signal to noise ratio in the experiment. Therefore, increasing the pump power input to the OPO is not always useful to further improve the photon pair generation rate. Here, we want to mention again that a diode laser is used in our experiment in contrast to the Ti:Sapphire in Ref. [50]. This small difference introduces some experimental differences. In our experiment, the output power of the ECDL is about 100 mW. Two 36-dB optical isolators have to be used to isolate the reflection from the optical components in order to protect the diode laser. The output power of 390-nm UV light in a single-pass SHG experiment is less than 40 μW. This power is too low to perform the SPDC experiment [22]. In order to get enough power at 390 nm, we realize the SHG with the aid of a cavity. One problem is that the spatial mode of the laser is very bad compared to the Ti:Sapphire laser, so we have to reform it by using a set of cylindrical lenses. This bad spatial mode also introduces one problem: the mode-matching between the pump mode and the cavity mode. In our experiment, two lenses are used to make the mode match between the pump mode and the cavity mode. There is a big problem concerning the operation of the cavity-based SHG experiment: the large absorption of the KTP crystal at less than 400-nm wavelength range. The absorption of the PPKTP crystal used is more than 20%, which induces the strong thermal lens effect. This makes the cavity unstable and finally reduces the output power. Therefore the maximal available power at 390-nm wavelength is only a few milliwatts in our experiment [22]. Another small difference between our experiment and the experiment in Ref. [50] is that an etalon is used to select a single mode output in Ref. [50]. In our experiment, we use a home-made cavity to select the single mode output. The cavity is also locked to the laser frequency by the PDH method.

We want to mention also that there are some works in which a type-I down-converter is used: in Ref. [53], the SPDC is done in a single pass configuration, and a narrow band filter is used to reduce the bandwidth of the

photon. In Ref. [16], two type-I converters are put in a ring cavity to generate a polarization entangled photon pair, but the output is multimode and therefore further filtering is necessary. It should be pointed out that a polarization entangled photon pair can be created by using the post-selection technology in Refs. [50–52], but it is not the case in our work, because a type-I phase matched SPDC is used in our work.

The single counts of both detectors are 22 000/s and 18 000/s respectively (with accidental counts). The count difference between two detectors is from the different coupling efficiencies to single mode fibers: one is about 80%, another is 60%. Another thing we want to point out is the relatively lower coincidence count to single count ratio and the large background noise shown in Fig. 20. We think it is mainly caused by the following: 1) all kinds of background lights, such as the reflected light from mirror and crystal; the leak light from the locking beam. Although a chopper is used to alternate the periods of the cavity locking and signal detection, it is still possible for leaking locking light; 2) The optical losses in our experimental setup, including the coupling loss of the photon pairs from the space to fiber, the non-unit detector efficiency; 3) The presence of the uncorrelated photons. These photons are from i) the multi-photon case and ii) fluorescence related to gray-tracking in KTP crystal. This kind of fluorescence originates from color-center formation which may be of the same order of magnitude in intensity as SPDC in a single-pass configuration.

Finally, we experimentally generate a narrow-band photon with a linewidth of 21 MHz, which is comparable to the typical linewidth of the Rb atom. This photon can be used to realize the storage and retrieval in Rb atomic ensemble, which is very important for long-distance quantum communication.

8 Conclusion

In an atomic-based network, the efficient coupling between a photon and an atomic system is a prerequisite for realizing the transfer of information between them, which requires that the photon has a comparable bandwidth with the natural bandwidth of an atom. Therefore, how to generate a narrow-band photon is a very important topic in the quantum information field. One simple and efficient way is based on the SPDC with a nonlinear crystal in a cavity. In this paper, we review and give a series of experiments done in our group for this goal. We finally achieve our goal and successfully generate narrow-band photons at 780-nm wavelength, which makes the storage and the retrieval of the photon in Rb atomic ensemble possible. We believe these results are very useful for the research in this direction.

Acknowledgements This work was supported by the National Natural Science Foundation of China (Grant Nos. 10674126 and 10874171), the National Basic Research Program of China (Grant Nos. 2006CB921900 and 2009CB929601), the Innovation fund from CAS, Program for NCET, and International Cooperate Program from CAS and Ministry of Science and Technology of China.

References

1. A. K. Ekert, Phys. Rev. Lett., 1991, 67: 661
2. C. H. Bennett and G. Brassard, in: Proceeding of the International Conference on Computers, Systems and Signal Processing Indian Institute of Science, India: Bangalore, 1984
3. A. Kuzmich, W. P. Bowen, A. D. Boozer, A. Boca, C. W. Chou, L. M. Duan, and H. J. Kimble, Nature, 2003, 423: 731
4. C. H. van der Wal, M. D. Eisaman, A. Andre, R. L. Walsworth, D. F. Phillips, A. S. Zibrov, and M. D. Lukin, Science, 2003, 301: 196
5. D. N. Matsukevich and A. Kuzmich, Science, 2004, 306: 663
6. D. C. Burnham and D. L. Weinberg, Phys. Rev. Lett., 1970, 25: 84
7. B. S. Shi and A. Tomita, Phys. Rev. A, 2004, 69: 013803
8. B. S. Shi and A. Tomita, Opt. Commun., 2004, 235: 247
9. B. S. Shi, F. Y. Wang, C. Zhai, and G. C. Guo, Opt. Commun., 2008, 281: 3390
10. B. Lounis and W. E. Moerner, Nature, 2000, 407: 491
11. V. Jacques, E. Wu, F. Grosshans, F. Treussart, P. Grangier, A. Aspect, and J. F. Roch, Science, 2007, 315: 966
12. C. Santori, D. Fattal, J. Vuckovic, G. S. Solomon, and Y. Yamamoto, Nature, 2002, 419: 594
13. X. S. Lu, Q. F. Chen, B. S. Shi, and G. C. Guo, Chin. Phys. Lett., 2009, 26: 064204
14. Q. F. Chen, B. S. Shi, M. Feng, Y. S. Zhang, and G. C. Guo, Opt. Express, 2008, 16: 21708
15. Z. Y. Ou and Y. J. Lu, Phys. Rev. Lett., 1999, 83: 2556
16. H. Wang, T. Horikiri, and T. Kobayashi, Phys. Rev. A, 2004, 70: 043804
17. C. E. Kuklewicz, F. N. C. Wong, and J. H. Shapiro, Phys. Rev. Lett., 2006, 97: 223601
18. M. Scholz, F. Wolfgramm, U. Herzog, and O. Benson, Appl. Phys. Lett., 2007, 91: 191104
19. F. Y. Wang, B. S. Shi, and G. C. Guo, Opt. Lett., 2008, 33: 2191
20. F. Y. Wang, B. S. Shi, and G. C. Guo, Opt. Commun., 2010, DOI: 10.1016/i.optcom.2010.02.042
21. X. S. Lu, Q. F. Chen, B. S. Shi, and G. C. Guo, Chin. Opt. Lett., 2009, 7: 1048
22. F. Y. Wang, B. S. Shi, Q. F. Chen, C. Zhai, and G. C. Guo, Opt. Commun., 2008, 281: 4114
23. F. Y. Wang, B. S. Shi, and G. C. Guo, Opt. Commun., 2010, 283: 551
24. F. Y. Wang, B. S. Shi, C. Zhai, and G. C. Guo, J. Mod. Opt., 2010, 57: 330
25. F. Torabi-Goudarzi and E. Riis, Opt. Commun., 2003, 227: 389
26. R. Le Targat, J. J. Zondy, and P. Lemonde, Opt. Commun.,

2005, 247: 471
27. F. Villa, A. Chiummo, E. Giacobino, and A. Bramatil., J. Opt. Soc. Am. B, 2007, 24: 576
28. G. R. Fayaz, M. Ghotbi, and Ebrahim-Zadeh, Appl. Phys. Lett., 2005, 86: 061110
29. A. A. Lagatsky, C. T. A. Brown, W. Sibbett, S. J. Holmgren, C. Canalias, V. Pasiskevicious, F. Laurell, and E. U. Rafailov, Opt. Express, 2007, 15: 1155
30. B. S. Shi and A. Tomita, J. Opt. Soc. Am. B, 2004, 21: 2081
31. S. Wang, V. Pasiskevicious, F. Laurell, and K. Karlsson, Opt. Lett., 1998, 23: 1883
32. W. Wiechmann, S. Kubota, T. Fukui, and H. Masuda, Opt. Lett., 1993, 18: 1208
33. J. D. Bierlein and H. Vanherzeele, J. Opt. Soc. Am. B, 1989, 6: 622
34. R. W. Drever, J. L. Hall, F. V. Kowalski, J. Hough, G. M. Ford, A. J. Munley, and H. Ward, Apply. Phys. B, 1983, 31: 97
35. G. Hansson, H. Karlsson, S. Wang, and F. Laurell, Appl. Opt., 2000, 39: 5058
36. S. Tanzilli, H. Reidmatten, W. Tittle, H. Zbinden, P. Baldi, M. De Micheli, D. B. Ostrowsky, and N. Gisin, Electron. Lett., 2001, 37(1): 26
37. K. Sanaka, K. Kawahara, and T. Kuga, Phys. Rev. Lett., 2001, 86: 5620
38. T. Kim, M. Fiorentino, and F. N. C. Wong, Phys. Rev. A, 2006, 73: 012316
39. A. B. U'Ren, C. Silerhorn, K. Bannaszek, and Ian A. Walmsley, Phys. Rev. Lett., 2004, 93: 093601
40. M. Pelton, P. Marsden, D. Ljunggren, M. Tengner, A. Karlsson, C. Canalias, and F. Laurell, Opt. Express, 2004, 12: 3573
41. A. Fedrizzi, T. Herbst, A. Poppe, T. Jennewein, and A. Zeilinger, Opt. Express, 2007, 15: 15377
42. O. Kuzucu and F. N. Wong, arXiv: quant-ph/0710.5390v1, 2007
43. B. S. Shi, C. Zhai, G. C. Guo, Y. K. Jiang, and A. Tomita, Opt. Commun., 2007, 278: 363
44. M. Fiorentino, S. M. Spillane, R. G. Beausoleil, T. D. Roberts, P. Battle, and M. W. Munro, Opt. Express, 2007, 15: 7479
45. H. Goto, Y. Yanagihara, H. B. Wang, T. Horikiri, and T. Kobayash, Phys. Rev. A, 2003, 69: 035801
46. C. K. Hong, Z. Y. Ou, and L. Mandel, Phys. Rev. Lett., 1987, 59: 2044
47. D. Bouwmeester, J. W. Pan, K. Mattle, M. Eibl, H. Weinfurter, and A. Zeilinger, Nature, 1997, 390: 575
48. J. W. Pan, D. Bouwmeester, H. Weinfurter, and A. Zeilinger, Phys. Rev. Lett., 1998, 80: 3891
49. Y. J. Lu and Z. Y. Ou, Phys. Rev. A, 2000, 62: 033804
50. X. H. Bao, Y. Qian, J. Yang, H. Zhang, Z. B. Chen, T. Yang, and J. W. Pan, Phys. Rev. Lett., 2008, 101: 190501
51. M. Scholz, L. koch, R. Ullmann, and O. Benson, Appl. Phys. Lett., 2009, 94: 201105
52. A. Haase, N. Piro, J. Eschner, and M. W. Mitchell, Opt. Lett., 2009, 34: 55
53. K. Akiba, K. Kashiwagi, M. Arikawa, and M. Kozuma, New J. Phys., 2009, 11: 013049